APPLICATION OF HIGH-RESOLUTION SCHEME IN ROTOR FLOW SIMULATION

Jianhua Xu*, Wenping Song* & Futian Xie**
***National Key Laboratory of Science and Technology on Aerodynamic Design and Research, School of Aeronautics, Northwestern Polytechnical University, Xi'an, China**
****China Aerodynamic Research and Development Center, Mianyang, China**

Email: jianhua19492002@163.com; wpsong@nwpu.edu.cn; wuhuiyuanming@sina.com

Keywords: *high-resolution scheme; helicopter rotor; multi-grid method*

Abstract

In this paper, the accuracy and efficiency of some high-resolution schemes including Roe and AUSM-type (Advection Upstream Splitting Method) in rotor flow simulation are investigated. Unsteady compressible Reynolds-Averaged Navier-Stokes equations in absolute coordinate system are utilized to simulate the rotor flow with a cell-centered finite-volume scheme. Moving chimera-grid methodology, fully implicit dual-time stepping method and multi-grid method are implemented for the simulation. In order to improve the efficiency and stability, a Newton-like LU-SGS (Lower-Upper Symmetric-Gauss-Seidel) scheme with viscous correction is applied to sub-iteration of dual-time stepping method. The viscous flow around Caradonna rotors in hover and forward flight are simulated by using presented high resolutions.

1 Background

The flow field around helicopter rotors is very complex. In hover flight, the blade-vortex interactions are significant; in forward flight, unsteady transonic effects which may induce shock waves or shock wave/boundary layer interaction are dominant on the advancing blade, while highly separated flow exists on the retreating blade, causing the dynamic stall. In addition, pitching, flapping and coning motions which are known as the rotor trimming problems further complicate the numerical simulations of the flow field in forward flight [1].

On the other hand, the prediction of helicopter rotor noise needs the accurate flow field data around the rotors especially for the computation of blade-vortex interaction (BVI) noise and high-speed impulsive (HSI) noise. A number of researchers have made a lot of efforts to improve the predicted accuracy of helicopter rotor noise. Recently, E.P.N Duque, etc. used advanced CFD methods including innovations in Large Eddy Simulation, novel techniques for flexible deforming blade, high-order methods for accuracy, and adaptive grids to accurately capture important flow features to modeling the noise characteristics of maneuvering rotorcraft [2]. In 2009, Futian Xie, etc. employed the low dissipation Roe scheme to calculate the flow around the rotors, including what is needed for predicting BVI noise in forward flight and demonstrated that Roe scheme helped to improve the prediction precision of BVI noise [3].

The main purpose of the work in this paper is introducing some high-resolution schemes including Roe and AUSM-type to simulate the flow around helicopter rotors in forward flight. In order to improve the efficiency, a full implicit dual-time stepping method and multi-grid method are utilized for the simulation. The viscous flow around Caradonna rotors in hover and forward flight are simulated, the accuracy and efficiency of these high-resolution schemes are compared to Jameson's central scheme.

2 Numerical Methods

2.1 Governing Equations

Three-dimensional Navier-Stokes equations in the inertial coordinate system and recast in absolute flow variables can be written as follows:

$$\frac{D}{Dt}\iiint_{\Omega}\mathbf{W}dV+\iint_{\partial\Omega}\overline{\overline{\mathbf{H}}}\bullet\mathbf{n}dS-\iint_{\partial\Omega}\overline{\overline{\mathbf{H}}}_{v}\bullet\mathbf{n}dS=0 \qquad (1)$$

where,

$$\frac{D}{Dt}\iiint_{\Omega}\mathbf{W}dV=\frac{\partial}{\partial t}\iiint_{\Omega}\mathbf{W}dV+\iint_{\partial\Omega}\mathbf{W}\mathbf{q}_{b}\bullet\mathbf{n}dS \qquad (2)$$

where, Ω is the control volume, $S,\mathbf{n}$ denote boundary of control volume and its unit-normal outer vector, respectively. $\overline{\overline{\mathbf{H}}}$ and $\overline{\overline{\mathbf{H}}}_{v}$ are inviscid flux vector and viscous flux vector, respectively. The flow variable vector is defined as:

$$W=[\rho,\rho u,\rho v,\rho w,\rho E]^{\mathrm{T}} \qquad (3)$$

ρ,u,v,w,E denote density, components of velocity vector and total energy per unit mass, respectively. $\mathbf{q}_{b}$ indicates the moving velocity for the boundary of control volume. For turbulent flow, Baldwin-Lomax algebraic turbulence model [4] or Spalart-Allmaras one – equation model [5] are used for turbulence enclosure.

A cell-centered finite-volume method developed by Jameson [6] is used to solve the governing equations. The fully implicit dual-time stepping method based on an improved Newton-like LU-SGS subiteration with second or three-order time accuacy is utilized for time stepping and a very efficient FAS multi-grid method on moving chimera grid is developed to improve the efficiency of sub-iteration. The detail of numerical method mentioned above can be found in Ref. [7] and [8].

2.2 Moving Chimera-grid Methodology and Boundary Conditions

Chimera grids based on three kinds of grid in the simulation are involved and demonstrated in Figs. 1-2. The background grid (H-H type) is for far-field computation, keeping absolutely stationary; the intermedial grid (H-H type) is for vortex capture, rotating with blades; the rotor grids (C-H type) are for viscous flow simulation, moving with blades that allows for prescribed pitching and flapping motion of rotor blades. The connection and information exchange between different grids are implemented by a very efficient and robust method based on a distance decreasing method [9].

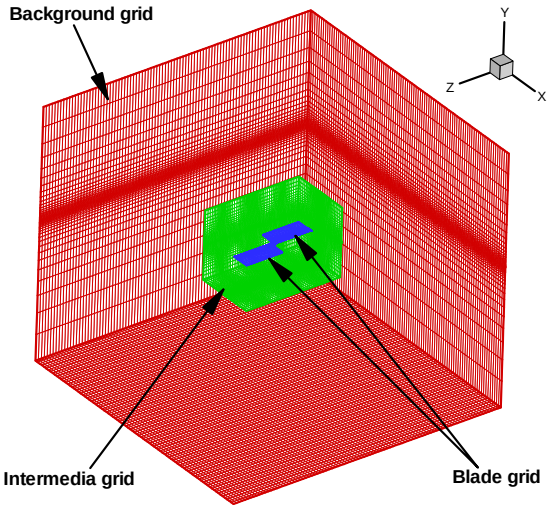

Fig. 1. Schematics of the Overall Topology of Overset Grids for Helicopter Rotor in forward flight

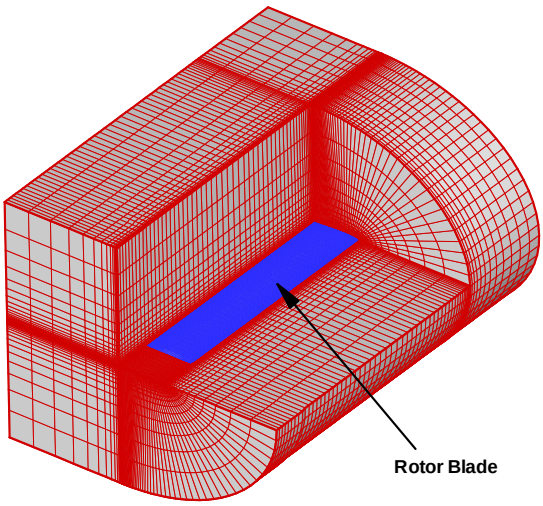

Fig. 2. The Room-in View of C-H Type Rotor Grid

For viscous flow, a no-slip boundary condition and adiabatic wall condition is enforced on the blade surface. That is the velocities of the surface grid points are consistent with the blade motion. One-dimensional approximate Riemann boundary conditions are applied at far-field boundaries (6 grid surfaces of background grid). Trilinear interpolation methodology is used to calculate the flow variables on fringe points and chimera boundary points.

2.3 Application of Multi-grid Method in Moving Chimera-grid Methodology

According to Ref. [10], there are 3 problems of multi-grid for chimera:

- Transfers between overlapped coarse grids;
- Blanking or not blanking points on coarse grids;
- Treatment of restriction and prolongation operators with blanked cells

Three transfer techniques on coarse grid for chimera are presented in the paper. Through the computations of airfoils and hovering rotors, the authors commended that extrapolation on points is implemented where interpolation cannot be used. Based on this, an improved method is developed in present paper [8]:

(1) Determine blanked points on coarse grid according to blanked points on fine grid. That is, if any one cell on coarse grid includes blanked points on fine grid, the cell is defined as a blanked point on coarse grid. Then, fringe points are determined according to these blanked points;

(2) Donor cells of fringe points and outer boundaries for chimera on coarse grids are searched on the finest grids themselves;

(3) A volume weighted method is used in corrections on coarse grid.

3 High-resolution Schemes

In this paper, several high-resolution numerical schemes are used to accurately capture vortexes and shocks.

For the governing equations in Eq. (1), the semi-discrete scheme can be written as follows:

$$\frac{D}{Dt}\left(\Omega_{i,j,k}\vec{Q}_{i,j,k}\right)+\hat{F}_{i,j,k}-\hat{F}_{v\,i,j,k}=0 \qquad (4)$$

where, $\vec{Q}$ are flow variables. $\hat{F}$ and $\hat{F}_v$ are inviscid and viscous flux, respectively.

For simplification, in the following descriptions of the high resolution schemes, the index i,j,k are not written, the subscript 1/2 stands for the quantities at a cell interface, L and R are subscripts for the quantities on the left and right of the cell interface.

3.1 Roe Scheme

Roe scheme is one of the earliest high-resolution numerical schemes [11]. A numerical expression of the inviscid flux vector by Roe scheme can be written as:

$$\hat{F}_{1/2}=\frac{1}{2}[\hat{F}_{1/2}(\vec{Q}_{\mathrm{L}})+\hat{F}_{1/2}(\vec{Q}_{\mathrm{R}})-|\tilde{A}|(\vec{Q}_{\mathrm{R}}-\vec{Q}_{\mathrm{L}})] \qquad (5)$$

$$|\tilde{A}|(\vec{Q}_{\mathrm{R}}-\vec{Q}_{\mathrm{L}})=\begin{bmatrix}\alpha_4\\ \tilde{u}\alpha_4+\hat{n}_x\alpha_5+\alpha_6\\ \tilde{v}\alpha_4+\hat{n}_y\alpha_5+\alpha_7\\ \tilde{w}\alpha_4+\hat{n}_z\alpha_5+\alpha_8\\ \tilde{h}_0\alpha_4+(\tilde{\tilde{U}}+V_{bn})\alpha_5+\tilde{u}\alpha_6+\tilde{v}\alpha_7+\tilde{w}\alpha_8-\dfrac{\tilde{a}^2\alpha_1}{\gamma-1}\end{bmatrix} \qquad (6)$$

where, $\vec{Q}$ are flow variables and $|\tilde{A}|$ is the Roe-averaged Jacobian matrix. The superscrip '~' denotes Roe-averaged quantities and h_0 is the total enthalpy, a is the sound speed. The definition of other variables in Eq. (6) can be referred in Ref [12].

3.2 AUSM-type Schemes

In 1993, Meng-Sing Liou proposed a new scheme named AUSM scheme, which has all the excellence of Roe scheme and Van Leer scheme, and eliminates their disadvantage. From then, a set of improvements are developed such as AUSM+, AUSMPW+, AUSMDV, and AUSM+_up, and so on. They are called AUSM-type schemes. In this paper, AUSMPW+ and AUSMDV schemes are used to simulate the flow around helicopter rotors.

For AUSM-type schemes, the inviscid interface flux $\hat{F}_{1/2}$ is split into a convective contribution $\hat{F}_{1/2}^{(c)}$ plus a pressure contribution $\hat{F}_{1/2}^{(p)}$.

$$\hat{F}_{1/2}=\hat{F}_{1/2}^{(c)}+\hat{F}_{1/2}^{(p)} \qquad (7)$$

3.2.1 AUSMPW$^+$ Scheme

AUSMPW+ scheme is an improved version of AUSMPW (AUSM by Pressure-Based Weight

Function). Reference [14] points out that, although AUSMPW has the merits, it contains a complicating function $f_{L,R}$, which entails extra computational costs. In AUSMPW+, $f_{L,R}$ is modified by considering accuracy, shock instability, and efficiency. It can be summarized as:

$$\hat{F}_{1/2} = \overline{M}_L^{+} a_{1/2} \vec{Q}_L + \overline{M}_L^{-} a_{1/2} \vec{Q}_R + \left(P_L^{+} \vec{p}_L + P_R^{+} \vec{p}_R\right) \quad (8)$$

where, $\vec{p}$ and a are pressure and numerical sound speed, and

(1) for $M_{1/2} \geq 0$

$$\begin{cases} \overline{M}_L^{+} = M_L^{+} + M_R^{-}\left((1-\omega)(1+f_R) - f_L\right) \\ \overline{M}_R^{-} = M_R^{-}\omega(1+f_R) \end{cases} \quad (9)$$

(2) for $M_{1/2} < 0$

$$\begin{aligned} \overline{M}_L^{+} &= M_L^{+}\omega(1+f_L) \\ \overline{M}_R^{-} &= M_R^{-} + M_L^{+}\left((1-\omega)(1+f_L) - f_R\right) \end{aligned} \quad (10)$$

where, $\omega(p_L, p_R) = 1 - \min\left(\frac{p_L}{p_R}, \frac{p_R}{p_L}\right)^3$, and function f is defined as:

$$f_{L,R} = \begin{cases} \dfrac{p_{L,R}}{p_s} - 1 & \left|M_{L,R}\right| \leq 1 \\ 0 & \textit{elsewhere} \end{cases} \quad (11)$$

where, $p_s = P_L^{+} p_L + P_R^{+} p_R$. Details are in [14].

3.2.2 AUSMDV Scheme

AUSMDV scheme is developed based on AUSM+ scheme [15]. The split Mach number and pressure functions for the two schemes are the same, and their difference is the chosen definition of quantity $m_{1/2}^{\pm}$.

For AUSM+,

$$\begin{cases} m_{1/2} = \boldsymbol{M}_{(4)}^{+}(M_i) + \boldsymbol{M}_{(4)}^{-}(M_{i+1}) \\ m_{1/2}^{\pm} = \dfrac{1}{2}\left(m_{1/2} \pm \left|m_{1/2}\right|\right) \end{cases} \quad (12)$$

For AUSMDV,

$$\begin{cases} m_{1/2}^{+} = \boldsymbol{M}_{(1)}^{+}(M_i) + \omega^{+}\left[\boldsymbol{M}_{(4)}^{+}(M_i) - \boldsymbol{M}_{(1)}^{+}(M_i)\right] \\ m_{1/2}^{-} = \boldsymbol{M}_{(1)}^{-}(M_{i+1}) + \omega^{-}\left[\boldsymbol{M}_{(4)}^{+}(M_{i+1}) - \boldsymbol{M}_{(1)}^{-}(M_{i+1})\right] \end{cases} \quad (13)$$

where,

$$\begin{aligned} \boldsymbol{M}_{(1)}^{\pm} &= \frac{1}{2}\left(M \pm |M|\right) \\ \boldsymbol{M}_{(4)}^{\pm} &= \begin{cases} \pm\frac{1}{4}(M \pm 1)^2 \pm \frac{1}{8}(M^2 - 1)^2 & |M| \leq 1 \\ \boldsymbol{M}_{(1)}^{\pm} & \textit{otherwise} \end{cases} \end{aligned} \quad (14)$$

$$\begin{aligned} \omega^{+} &= \left(\frac{p_i}{\rho_i}\right) \Bigg/ \left(\left[\frac{1}{2}\left(\frac{p_i}{\rho_i} + \frac{p_{i+1}}{\rho_{i+1}}\right)\right]\right) \\ \omega^{-} &= \left(\frac{p_{i+1}}{\rho_{i+1}}\right) \Bigg/ \left[\frac{1}{2}\left(\frac{p_i}{\rho_i} + \frac{p_{i+1}}{\rho_{i+1}}\right)\right] \end{aligned} \quad (15)$$

Details are given in Ref. [15] and [16].

4 Results and Discussion

A model rotor test, conducted by Caradonna [17] et al, in 1981, is selected for the present research. The model rotor utilized an NACA 0012 airfoil section with straight, untwisted blades. The rotor radius was 1.142 m with a chord of 0.1905 m.

In present work, the background grid contains 423801 points ($93\times49\times93$), the intermedial grid contains 414129 points ($73\times61\times93$) and the blade grid contains 407745 points ($153\times41\times65$). For all the computations, 180 steps per period are chosen for the marching of real time and the sub-iteration number of 50 is taken for the marching in pseudo time. All the computations are run on the PC with 2.4GHz Intel Core CPU and 3G memory.

4.1 Hover Flight

For the hover flight case, the tip Mach number $Ma_{Tip} = 0.877$, the blade pitch angle $\theta = 8^{o}$ and the Reynolds number $\mathrm{Re} = 3.93\times10^{6}$. Fig. 3 shows pressure contour of blade surface calculated by Jameson's central scheme (JST) and Roe scheme. It demonstrates that sharper shock is captured by using Roe scheme. Fig. 4 and Fig. 5 show pressure distributions calculated with the two schemes and that of experimental data. It indicates that Roe scheme results in higher resolution in shock capturing,

and the pressure distributions are more consistent with that of experimental data.

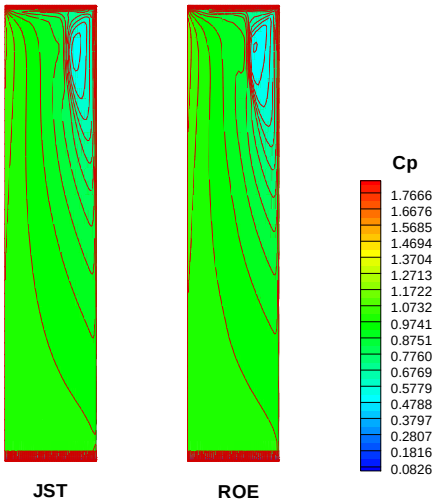

Fig. 3. Pressure Contour by Different Schemes

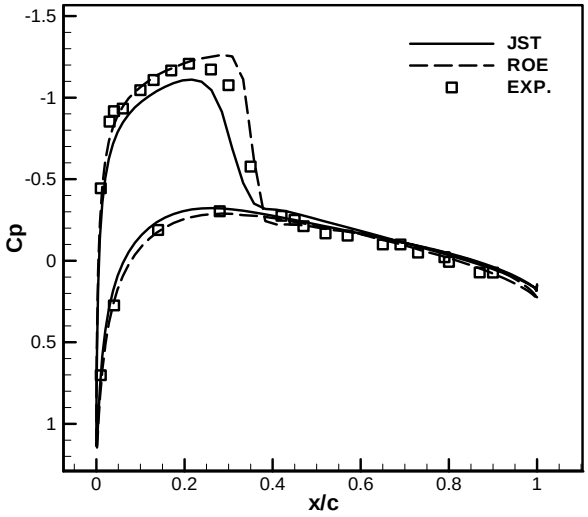

Fig. 4. Pressure Distribution (r/R=0.89)

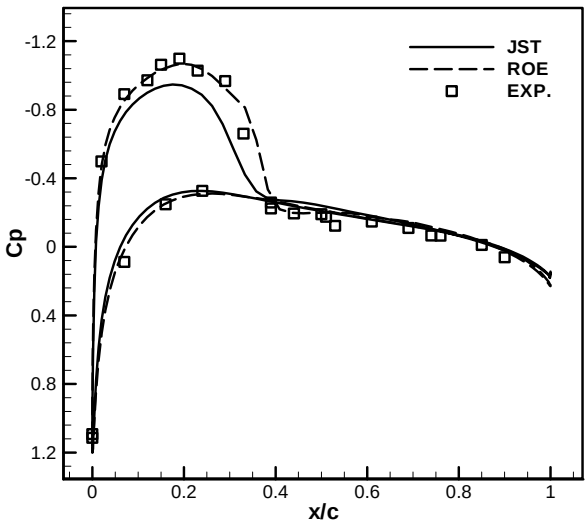

Fig. 5. Pressure Distribution (r/R=0.96)

4.2 Forward Flight

In the forward flight case, the tip Mach number $Ma_{Tip} = 0.628$, the blade pitch angle $\theta = 8^o$, the advanced ratio $\lambda = 0.3$ and the Reynolds number $\mathrm{Re} = 3.66 \times 10^6$. The unsteady computations are completed when the third cycle is finished and periodical solutions are obtained. Fig. 6 and Fig. 7 demonstrate pressure distributions of four different schemes and experimental data at r/R=0.80 and r/R=0.96 where the azimuth angle $\Phi = 90^o$, where sharp shocks exist. All the three high-resolution schemes obtain almost the same solution, especially higher accuracy in shock capturing than JST scheme. It can be concluded that the accuracy of Roe scheme and AUSM-type

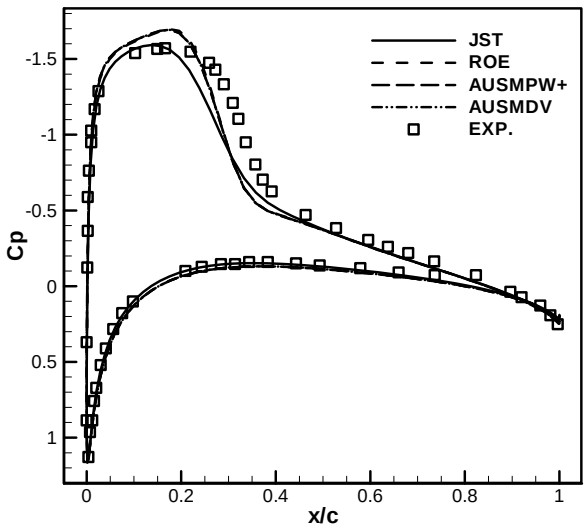

Fig. 6. Pressure Distribution ($\Phi = 90^o$, r/R=0.80)

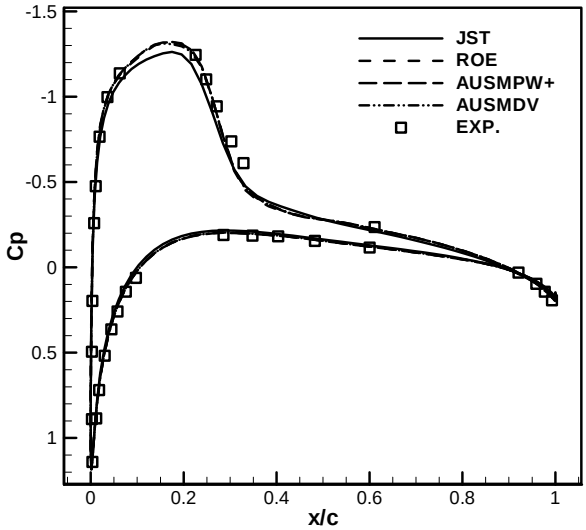

Fig. 7. Pressure Distribution ($\Phi = 90^o$, r/R=0.96)

schemes is equivalent.

In this case, a study on the efficiency of multi-grid method is made. Tab. 1 and Tab. 2 show efficiency of different multi-grid cycles for the four schemes. Obviously, the acceleration ratio of sub-iteration number reaches 2.0, but the acceleration ratio of CPU time is low. Most interestingly, for multi-grid computations, 2-level cycle needs a little less total sub-iteration number and CPU time than that of 3-level's.

Tab. 1 Total sub-iteration number for different multi-grid cycles

Scheme	Single grid	Multigrids 2 levels	Multigrids 3 levels
JST	5277	2167	2339
Roe	6281	3007	3568
AUSM PW+	6811	3489	3912
AUSM DV	6763	3420	3845

Tab. 2 Total CPU time (hours) for different multi-grid cycles

Scheme	Single grid	Multigrids 2 levels	Multigrids 3 levels
JST	22.31	13.80	15.25
Roe's	27.87	21.16	26.83
AUSM PW+	29.92	24.42	28.26
AUSM DV	29.71	23.92	28.72

5 Conclusions

Some high-resolution schemes are developed and investigated for rotor flow simulation. Full implicit dual-time stepping method and multi-grid method are utilized to improve the accuracy and efficiency. The study made in the present work can be summarized as following:

(1) The accuracy of Roe and AUSM-type schemes is equivalent;

(2) For high resolution schemes, the efficiency of Roe scheme is higher than AUSM-type schemes.

(3) For multi-grid computations, 2-level cycle needs a little less total sub-iteration number and CPU time than that of 3-level's.

6 Acknowledgments

The research is funded by the Science and Technical Foundation of Chinese National Key Laboratory of Science and Technology on Aerodynamic Design and Research (9140C4201020802). Jianhua Xu thanks Dr. Zhonghua Han for sharing his technical material and experience in rotor flow simulations and for many useful technical discussions.

References

[1] R. Steijl, G.N. Barakos and K.J. Badcock. A CFD Framework for Analysis of Helicopter Rotors. AIAA Paper 2005-5124, 2005.

[2] E.P.N Duque, L.N Sankar, S. Menon, etc. Revolutionary Physics-Based Design Tools for Quiet Helicopters. AIAA Paper 2006-1068, 2006.

[3] Xie Futian, Song Wenping and Han Zhonghua. A method Based on Low Dissipation Roe Scheme and RANS Equations for Predicting BVI Noise of Helicopter Rotor in Forward Flight. *Journal of Northwestern Polytechnical University*, Vol. 27, No. 2, pp 151-156, 2009.

[4] Baldwin B and Lomax H. Thin Layer Approximation and Algebraic Model for Separated Turbulent Flow. AIAA Paper 1978-257, 1978.

[5] Spalart P. R. and Allmaras S. R. A One Equation Turbulence Model for Aerodynamic Flows. AIAA 92-0439, 1992.

[6] Jameson A, Schmidt W and Turkel E, Numerical Solutions of the Euler Equations by a Finite Volume Method using Runge-Kutta Time Stepping Schemes. AIAA Paper 1981-1259, 1981.

[7] Qiao Z.D., Yang A.M. and Zhu, B., Computation of the Unsteady Viscous Flow about Helicopter rotors in Forward Flight by a Full Implicit Dual Time Method. AIAA Paper 2003-4082, 2003.

[8] Han Z.H., Efficient Method for Simulation of Viscous Flows past Helicopter Rotors and Active Flow Control (PHD). Xi'an: Northwestern Polytechnical University, 2007.

[9] Yang Wenqing, Song Bifeng and Song Wenping. Distance Decreasing Method for Confirming Corresponding Cells of Overset Grids and Its Application. *Acta Aeronautica Et Astronautica Sinica*, Vol. 30, No. 2, pp 205-212, 2009.

[10] Xavier Juvigny, Elodie Canonne and Christophe Benoit. Multigrid Algorithms for the Chimera Method. AIAA Paper 2004-758, 2004.

[11] Roe P L, Approximate Riemann Solver, Parameter Vectors, and difference schemes. *Journal of Computational Physics*, Vol.43, No. 2, pp 357-372, 1981.

[12] Chen, C. L. and McCroskey, W. J., Numerical Solutions of Forward Flight Rotor Flow Using An Upwind Method. AIAA Paper 89-1846, 1989.

[13] Frink N. T., Parikh P. and Pirzadeh S., A Fast Upwind Solver for the Euler Equations on Three-Dimensional Unstructured Meshes. AIAA Paper 91-0102, 1991.

[14] Kim, K. H., Kim, C., and Rho, O. H., Methods for the Accurate Computations of Hypersonic Flows: I. AUSMPW+ Scheme. *Journal of Computational Physics*, Vol. 174, No. 1, pp 38–80, 2001.

[15] Meng-Sing Liou, A sequel to AUSM: AUSM+. *Journal of Computational Physics*, Vol.129, No. 2, pp: 364~382, 1996.

[16] Meng-Sing Liou and Jack R. Edwards, Low-Diffusion Flux-Splitting Methods for Flows at All Speeds. AIAA Paper 97-1862, 1997.

[17] Caradonna F X and Tung C. Experimental and analytical studies of a model helicopter rotor in hover. Vertica. NASA TM-81232, 1981.

[18] Yang Wenqing, Song Bifeng and Song Wenping. Distance Decreasing Method for Confirming Corresponding Cells of Overset Grids and Its Application. *Acta Aeronautica Et Astronautica Sinica*, Vol. 30, No. 2, pp 205-212, 2009.

Copyright Statement